

Self-consistent calculations of electron-capture decays in $Z=118$, 119, and 120 superheavy isotopes

P. Sarriguren

Instituto de Estructura de la Materia, IEM-CSIC, Serrano 123, E-28006 Madrid, Spain

Abstract

Weak decays in superheavy nuclei with proton numbers $Z = 118 - 120$ and neutron numbers $N = 175 - 184$ are studied within a microscopic formalism based on deformed self-consistent Skyrme Hartree-Fock mean-field calculations with pairing correlations. The half-lives of β^+ decay and electron capture are compared with α -decay half-lives obtained from phenomenological formulas. The sensitivity of the half-lives to the unknown Q -energies is studied by comparing the results obtained from different approaches for the masses. It is shown that α -decay is always dominant in this mass region. The competition between α and β^+/EC decay modes is studied in seven α -decay chains starting at different isotopes of $Z=118$, 119, and 120.

Keywords: Weak-decay half-lives; superheavy nuclei; nuclear density-energy functional

1. Introduction

The last decades have witnessed a lot of progress in the search and discovery of increasingly heavy elements and it is nowadays a very fruitful line of research [1, 2, 3, 4, 5]. Superheavy nuclei (SHN) with $Z = 107 - 113$ were synthesized from cold-fusion reactions by using target nuclei ^{208}Pb and ^{209}Bi and medium-mass stable isotopes of Ti, Cr, Fe, Ni, and Zn as projectiles [1, 2, 6]. Production of heavier elements from these reactions were difficult because of the strong Coulomb repulsion for increasing charge of the projectiles. Then, hot-fusion reactions involving long-lived actinide nuclei from ^{238}U to ^{249}Cf as targets and the double magic nucleus ^{48}Ca as projectiles were carried out to produce SHN with $Z=112-118$ in the neutron-evaporation (xn) channels [2, 7, 8, 9]. As a consequence of these experimental campaigns all the elements with $Z \leq 118$ have been discovered.

However, theoretical macroscopic-microscopic models [10, 11, 12] that include self-consistent treatments of the shell corrections [13, 14, 15, 16, 17], predict new regions of particularly stable nuclear systems with proton shells closures at $Z = 114, 120, 124$ or 126 and neutron shell closures at $N = 172, 184$, depending on the interactions and parametrizations used. Since no clear indications of closed shell at $Z = 114$ or $N = 172$ have been observed, there is a strong motivation for the search of more neutron-rich isotopes, as well as of heavier elements in an attempt to get closer to the predicted regions of stability. Concerning superheavy neutron-rich isotopes, alternative ways for their production are being explored [18, 19, 20] through fusion-evaporation reactions that include not only xn channels,

but also the emission of charged particles from the compound nucleus in the pxn and αxn channels, as well as through multinucleon transfer reactions or fusion reactions with radioactive ion beams [21]. The production of elements beyond oganesson requires complete fusion reactions with projectiles with $Z > 20$ because of the insufficient amounts of actinide targets with $Z > 98$ available [4, 22]. Different possibilities of projectiles (^{50}Ti , ^{54}Cr , ^{58}Fe , ^{64}Ni) and targets (^{249}Cf , ^{248}Cm , ^{244}Pu , ^{238}U) have been recently studied, both experimentally and theoretically, in a search for the most suitable combination to produce elements with $Z > 118$. Albers et al. [23] have measured mass and angle distributions of fission fragments for several reactions, concluding that $^{50}\text{Ti} + ^{249}\text{Cf}$ has the highest fusion probability among the reactions studied and thus, is the best candidate for the formation of $Z = 120$. Similarly, Adamian et al. [24] found within a microscopic-macroscopic approach that, among the reactions studied, $^{50}\text{Ti} + ^{249}\text{Bk}$ and $^{50}\text{Ti} + ^{249}\text{Cf}$ have the largest cross section for the production of evaporation residues with $Z = 119$ and $Z = 120$, respectively.

The stability of the compound nuclei in the superheavy region is generally determined by spontaneous fission. However, near the predicted islands of stability, fission barriers increase because of associated effects of shell closures and the half-lives of spontaneous fission may increase dramatically as shown in Ref. [25]. This enables other radioactive decay modes, such as α -decay or weak decays, that may come into play. In particular, the β^+/EC -decay in SHN may open new pathways towards the predicted region of stability [26, 27]. This possibility is also being studied experimentally [28, 29]. Theoretical predictions of weak decays are based on different approaches.

Email address: p.sarriguren@csic.es (P. Sarriguren)

Phenomenological parametrizations [30] have been developed that can be used to extrapolate to regions where the β^+/EC half-lives are unknown. There are also calculations that neglect nuclear structure effects, such as those in Refs. [26, 27, 31, 32], where only transitions connecting parent and daughter ground states are considered. The nuclear matrix elements of these transitions were assumed to be a constant value phenomenologically determined and valid for all nuclei. However, this value can vary by almost two orders of magnitude (from $\log(ft) = 4.7$ up to $\log(ft) = 6.5$), depending on the reference. In a different approach, half-lives for β^+/EC -decay were also evaluated within a proton-neutron quasiparticle random-phase approximation (pnQRPA) based on a phenomenological folded-Yukawa single-particle Hamiltonian [33].

Following the work started in Refs. [34, 35], we study here the β^+/EC -decay half-lives of some selected even-even and odd- A isotopes with $Z = 118 - 120$ and $N = 175 - 184$ and the competition with α -decay. The production of new elements with $Z = 119$ and 120 is one of the main objectives at worldwide leading laboratories such as SHI-GSI and FLEROV-JINR-DUBNA. Therefore, the study in this work addresses a highly topical issue. Furthermore, a comparison between α and β^+/EC -decay modes is made for seven α -decay chains that follow the production of isotopes with $Z=118, 119$, and 120 . The method of calculation of the weak decays is based on the pnQRPA approach with a microscopic nuclear structure calculation consisting on a deformed self-consistent Hartree-Fock calculation with Skyrme interactions and pairing correlations in the BCS approximation (HF+BCS).

2. Theoretical formalism

The microscopic approach used in this work to calculate β^+/EC -decay half-lives is presented here. The method follows closely the theoretical formalism used in Ref. [34, 35] for SHN. Further details of the formalism can be found elsewhere [36, 37].

The β^+/EC -decay half-life, $T_{\beta^+/EC}$, is calculated by summing all the allowed Gamow-Teller (GT) transition strengths connecting the parent ground state with states in the daughter nucleus with excitation energies, E_{ex} , lying below the Q_i energy ($i = \beta^+, EC$) and weighted with phase-space factors $f^i(Z, Q_i - E_{ex})$,

$$T_{1/2,i}^{-1} = \frac{(g_A/g_V)_{\text{eff}}^2}{D} \sum_{0 < E_{ex} < Q_i} f^i(Z, Q_i - E_{ex}) B(GT, E_{ex}), \quad (1)$$

with $D = 6143$ s and $(g_A/g_V)_{\text{eff}} = 0.77(g_A/g_V)_{\text{free}}$, where 0.77 is a standard quenching factor and $(g_A/g_V)_{\text{free}} = -1.270$. Therefore, the basic pieces of the calculation are the energies Q_i , the phase-space factors f^i and the GT strength distribution $B(GT, E_{ex})$.

Q_i energies are crucial to evaluate the half-lives because they determine the maximum energy of the transition and the values of the phase factors that weight the GT strength. They are defined in terms of the nuclear masses $M(A, Z)$ and the electron mass m_e ,

$$Q_{EC} = Q_{\beta^+} + 2m_e = M(A, Z) - M(A, Z - 1) + m_e. \quad (2)$$

Usually, one takes experimental masses to evaluate Q_{EC} , but in the case of the SHN studied here the masses have not been determined yet. Therefore, one has to rely on theoretical predictions for them. There is a large number of mass formulas available, which have been obtained from different approaches. We have considered in this work a selection of these mass formulas to evaluate the sensitivity of the half-lives to the unknown Q -energies. This breaks the self-consistency of the microscopic calculation, but provides a measure of the uncertainties involved in the calculated half-lives.

Among the pure phenomenological approaches for the masses, the Weizsacker-Bethe (WB) nuclear mass formula [38] is used. Several macroscopic-microscopic models are also considered. Among them we use the finite-range droplet model (FRDM) [39], which is corrected with microscopic effects obtained from a deformed single-particle model based on folded-Yukawa potentials including pairing in the Lipkin-Nogami approach and the nuclear mass formula of Ref. [40] (KTUY) that combines a gross term describing the general trend of the masses, an even-odd term, and a shell correction term describing the deviations of the masses from the general trend. The Duflo and Zuker (DZ-10) mass model [41], which is written as an effective Hamiltonian that contains monopole and multipole terms, is used as well. Another macroscopic-microscopic mass formula inspired by the Skyrme energy-density functional is also considered. In particular, we use the Weizsacker-Skyrme formula WS4 that includes a surface diffuseness correction for unstable nuclei and radial basis function corrections (WS4+RBF) [42]. This mass formula has been shown to be very reliable describing SHN [43]. Finally, we also compare with fully microscopic calculations based on effective two-body Skyrme nucleon-nucleon interactions by using the masses from the Skyrme forces SkM* and SLy4 with a zero-range pure volume pairing force [44] and Lipkin-Nogami method obtained from the code HFBTHO [45]. Tables for these masses can be found on websites [46].

Figure 1 shows the Q_{EC} energies for the isotopes with $Z = 118, 119, 120$ obtained from the mass formulas mentioned above. It also contains (black solid circles) the average values for each isotope. The results for each isotope are typically distributed around 2 MeV. Similarly, Fig. 2 shows the Q_α energies, $Q_\alpha = M(A, Z) - M(A - 4, Z - 2) - M(4, 2)$, calculated with the same mass formulas. They show a similar spread of the results.

The phase-space factors contain two components, positron emission f^{β^+} and electron capture f^{EC} . They

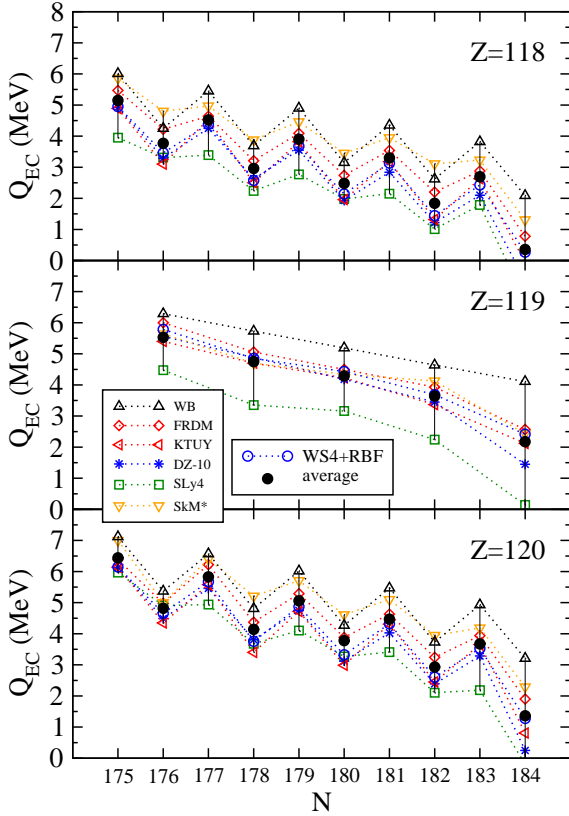


Figure 1: Q_{EC} energies (MeV) corresponding to different calculated masses for $Z = 118, 119,$ and 120 isotopes.

are computed numerically for each value of the energy using the code LOGFT, as explained in Ref. [47].

$$f^{\beta^+}(Z, W_0) = \int_1^{W_0} pW(W_0 - W)^2 \lambda^+(Z, W) dW, \quad (3)$$

with

$$\lambda^+(Z, W) = 2(1 + \gamma)(2pR)^{-2(1-\gamma)} e^{-\pi y} \frac{|\Gamma(\gamma + iy)|^2}{[\Gamma(2\gamma + 1)]^2}, \quad (4)$$

where $\gamma = \sqrt{1 - (\alpha Z)^2}$; $y = \alpha ZW/p$; α is the fine structure constant and R the nuclear radius. W is the total energy of the β particle, W_0 is the total energy available and $p = \sqrt{W^2 - 1}$ is the momentum.

The electron capture phase factors, f^{EC} , are given by

$$f^{EC} = \frac{\pi}{2} \sum_x q_x^2 g_x^2 B_x, \quad (5)$$

where x denotes the atomic sub-shell from which the electron is captured that includes K - and L - orbits. q is the neutrino energy, g is the radial component of the bound-state electron wave function at the nuclear surface, and B stands for other exchange and overlap corrections [47] that come from the indistinguishability of the electrons and from the decrease of the nuclear charge by one unit during

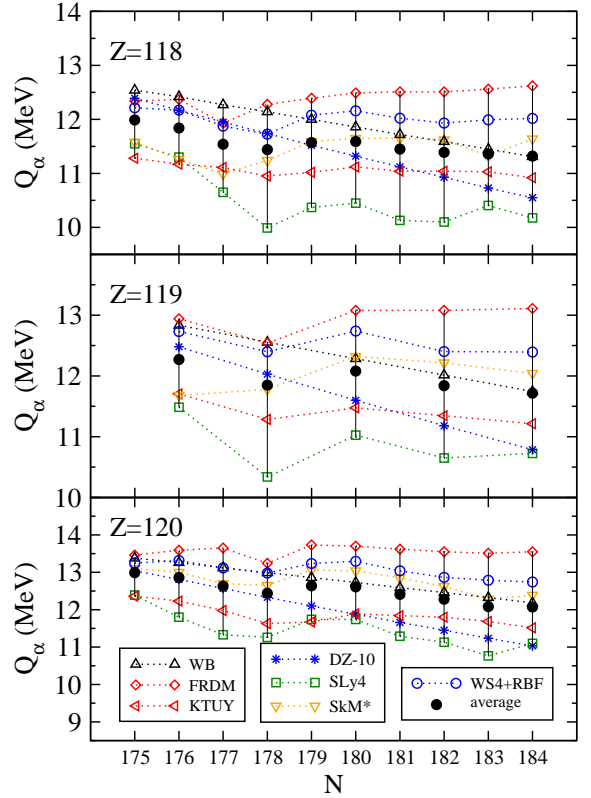


Figure 2: Same as in Fig. 1, but for Q_α energies.

the decay, respectively. The bound-state radial wave functions and the correction factors are obtained from a relativistic self-consistent mean-field calculation. They are solutions of the Dirac equation with a Hartree self-consistent potential and exchange terms included in the Slater approximation [48]. The nuclear potential corresponds to a finite-size nucleus with a Fermi distribution for the nuclear charge density.

Various improvements have been implemented recently to calculate more accurately the phase space factors. They have led to a more precise evaluation of the theoretical half-lives for β -decay and electron captures [49, 50]. The final result found in these works is a small correction of a few percent with respect to standard calculations in the framework of ref. [47]. This may be quite important in some specific cases when comparing with very precise experimental data, but it is irrelevant in this case, where the purpose is to compare half-lives of different decay processes that differ by several orders of magnitude, as we shall see later. This change is also irrelevant when compared to the change induced by other uncertainties studied in this work, such as the unknown Q_{EC} energies. Therefore, the use of more accurate electron wave functions will not change the main conclusion of this work regarding the competition between α and β decay modes.

The nuclear structure involved in the β^+/EC -decay is contained in the energy distribution of the GT strength $B(GT, E_{ex})$. At variance with other approaches mentioned

earlier to calculate $T_{\beta^+/\text{EC}}$ in SHN, we use in this work a microscopic approach. We start with a self-consistent calculation of the mean field by means of a deformed Hartree-Fock procedure with Skyrme interactions and pairing correlations in the BCS approximation. This calculation provides us single-particle energies, wave functions, and occupation probabilities. The Skyrme interaction SLy4 [51] is chosen for this study because of its proven ability to describe successfully nuclear properties throughout the entire nuclear chart [44]. The solution of the HF equations is found by using the formalism developed in Ref. [52], under the assumption of time reversal and axial symmetry. The single-particle wave functions are expanded in terms of the eigenstates of an axially symmetric harmonic oscillator in cylindrical coordinates using 16 major shells, after verifying that this size is large enough to get convergence of the HF energies. Deformation-energy curves (DECs) are constructed by constrained HF calculations that allow to analyze the nuclear binding energies as a function of the quadrupole deformation parameter β_2 . The profiles of these curves are found to converge with the basis used. Furthermore, eventual truncation errors become largely cancelled out when subtracting energies between the two decay partners to calculate Q-values.

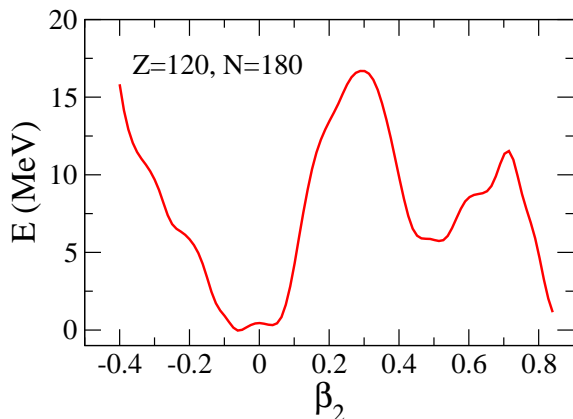


Figure 3: Deformation-energy curve for the $^{300}_{120}$ isotope obtained from constrained HF+BCS calculations with the Skyrme force SLy4.

Figure 3 shows the DEC of the isotope $^{300}_{120}$ as a representative example of the nuclei in this mass region. The energy in Fig. 3 is relative to the ground state energy. The results show a ground state corresponding to an almost spherical shape, as well as an excited prolate minimum at $\beta_2 \approx 0.5$. The profile of the DEC turns out to be very similar to the DEC obtained for the other isotopes discussed in this work and agree also quite well with calculations performed with the finite-range Gogny D1S interaction [53]. In this work we calculate energy distributions of the GT strength and their corresponding half-lives for the ground state configurations at $\beta_2 \approx -0.05$, as well as for the prolate configuration at $\beta_2 \approx 0.5$ that might be populated in the de-excitation of the compound nucleus. Nuclear deformation has been shown to be a key ingredient to describe

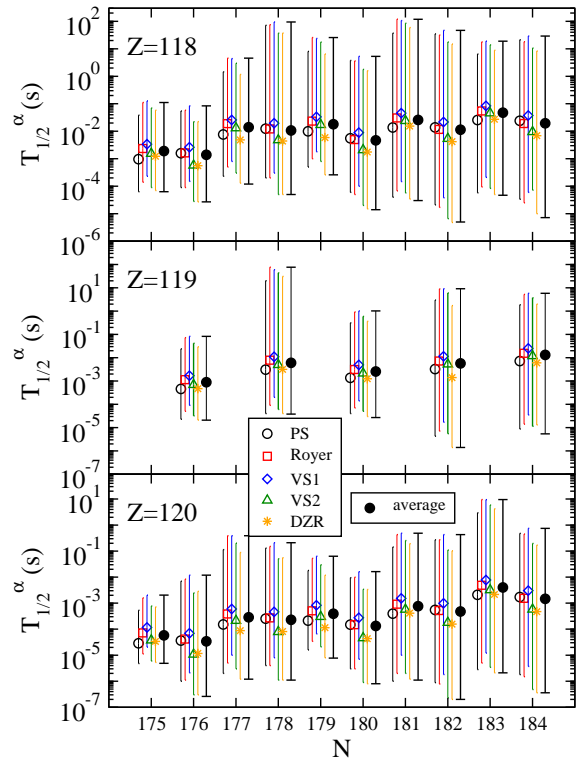


Figure 4: Calculated α -decay half-lives for $Z = 118, 119,$ and 120 isotopes for five different phenomenological formulas of T_{α} , namely, PS [68], Royer [69], VS1 [70], VS2 [26, 71], and DZR [72] and their average value.

β -decay properties in many different mass regions [36, 37] and it is also expected to play a significant role in SHN [34, 35]. A deformed pnQRPA with residual spin-isospin interactions is used to obtain the energy distribution of the GT strength needed to calculate the half-lives. In the case of SHN the coupling strengths of the residual interactions that scale with the inverse of the mass number are expected to be very small and their effect is neglected.

In the case of odd- A nuclei the procedure followed is based on the blocking of a given state with a given spin and parity, using the equal filling approximation to calculate its nuclear structure [37]. This approximation has been shown to be sufficiently precise for most practical applications [54]. The blocked state is chosen among the states in the vicinity of the Fermi level as the state that minimizes the energy.

This model of nuclear structure has been successfully used in the past to calculate weak-decay properties in different mass regions including neutron-deficient medium-mass [55, 56] and heavy nuclei [57, 58, 59], neutron-rich nuclei [60, 61, 62, 63, 64], and fp -shell nuclei [65, 66]. The effect of various ingredients of the model like deformation and residual interactions on the GT strength distributions, which finally determine the decay half-lives, was also studied in the above references. In particular, the sensitivity of the GT distributions to deformation has been used to learn about the nuclear shapes when comparing with ex-

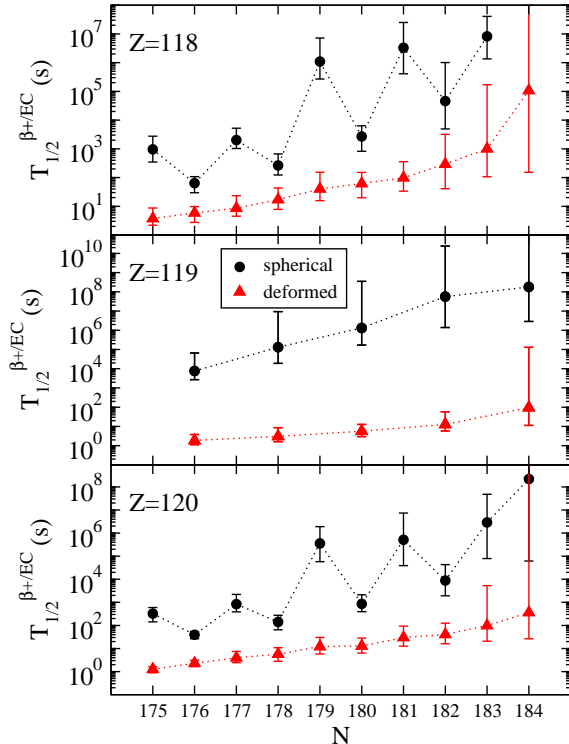


Figure 5: Calculated β^+/EC -decay half-lives for $Z = 118, 119,$ and 120 isotopes, using the average, maximum, and minimum Q_{EC} values in Fig. 1. Results for the ground-state spherical and excited prolate deformed shapes are shown.

periment [67].

3. Half-lives: Results and discussion

Comparison between α - and β^+/EC -decay modes is crucial to understand the possible branching and pathways of the original compound nucleus leading to stability.

Since no experimental information is still available on the α -decay half-lives (T_α), one has to rely on phenomenological formulas, which in turn depend on the unknown Q_α values. Thus, to get an idea of the spread of the results on T_α expected from uncertainties in both Q_α energies and phenomenological formulas of T_α , we have calculated the half-lives from five parametrizations and seven mass formulas, as well as the average, maximum, and minimum values.

Following the same approach as in Ref. [34], several parametrizations are used, which were fitted to account for the properties of SHN. Namely, they are the formula by Parkhomenko and Sobiczewski [68] (PS), the Royer formula [69] (Royer), and the Viola-Seaborg formula [70] with parameters from [68] (VS1) and [26, 71] (VS2). In addition to these formulas we also consider here a recent formula [72] (DZR) that takes into account both the blocking effect of the unpaired nucleon and the contribution of the centrifugal potential. This is an improvement of the Royer formula, which is simpler and more accurate.

Figure 4 contains the results for T_α . The values shown with different symbols and colors correspond to calculations from the five different parametrizations using the average values of Q_α (see Fig. 2). The error bars for each calculation correspond to the use of the maximum and minimum Q_α values predicted by the different mass evaluations. Solid black circles correspond to the average values of the five formulas. Their vertical lines join the maximum and minimum values obtained from the different $T_\alpha(Q_\alpha)$ alternatives. While the predictions of different parametrizations are within one order of magnitude, the uncertainties originated from the Q_α energies may vary up to seven orders of magnitude.

Figure 5 contains the results for $T_{\beta^+/EC}$ calculated with the formalism described in the previous section. The results plotted with a symbol (circle or triangle) correspond to the use of the average values of Q_{EC} in Fig. 1. The maximum and minimum values of $T_{\beta^+/EC}$ for each isotope correspond to the minimum and maximum values of Q_{EC} , respectively, according to the different mass formulas. They are plotted as error bars that join these extreme values, giving a measure of the uncertainties associated with the unknown Q_{EC} energies.

The results with black circles correspond to the slightly oblate, almost spherical, ground states ($\beta_2 \approx 0$), whereas the red triangles stand for the results from the deformed prolate shapes ($\beta_2 \approx 0.5$). Clearly, the half-lives from deformed shapes are much lower than those from spherical shapes for a given isotope. The reason of this behavior can be traced back to the different scenarios in the deformed or spherical cases having very different density of levels. In the β^+/EC -decay one proton is transformed into one neutron. The low-lying excitations below Q_{EC} in the daughter nucleus that finally determine the half-lives come from transitions connecting protons around the Fermi level for $Z = 118 - 120$ with neutrons around the Fermi level in the mass region $N = 175 - 184$. In a pure spherical approach, the GT operator should match protons from the spherical shell $2f_{5/2}$ of negative parity with neutrons from the $2g_{7/2}, 3d_{3/2}, 3d_{5/2}, 4s_{1/2}$ shells, which are positive parity states. Thus, these transitions will be very suppressed in nuclei with small deformations because of parity arguments. On the other hand, in the deformed case, many different orbitals from different spherical shells with positive and negative parity cross each other leading to a much more mixed scenario where states with both parities are found in the vicinity of the Fermi levels of protons and neutrons. The final result is an enhancement of the GT strength at low energy that leads to a shorter half-life in the case of deformed nuclei.

Another interesting observation is the existence of an odd-even staggering effect in the spherical case, which does not appear in the deformed case. This peculiar behavior is related to the characteristics of the excitations in the odd nuclei. The low-lying transitions in the odd system correspond basically to one-quasiparticle (1qp) excitations where the odd nucleon is involved in the pro-

cess. At higher excitation energies, typically beyond the energy needed to break a pair of nucleons, the transitions are mainly three-quasiparticle (3qp) excitations similar to those in the even-even system but with the odd nucleon acting as a spectator. For nuclei in this mass region, which have rather small Q_{EC} energies, the 3qp excitations are shifted in energy beyond Q_{EC} , while the low-lying 1qp excitations connecting protons from the $2f_{5/2}$ shell with neutrons in the $2g_{7/2}$, $3d_{3/2}$, $3d_{5/2}$, $4s_{1/2}$ shells are very suppressed because of parity. The final result for spherical nuclei is that in the odd nuclei very little strength remains within the Q_{EC} window giving rise to quite large half-lives as compared with the even-even nuclei. In the deformed case this effect is not manifest because of the higher level density around the Fermi levels that involve states with both positive and negative parities, as well as many angular momentum components.

Comparing the half-lives in Figs. 4 and 5, one can see that the β^+/EC -decay half-lives are systematically several orders of magnitude larger than the corresponding average α -decay half-lives for a given isotope. The range of this difference is between three and five orders of magnitude in the deformed case and even larger in the spherical one. Only when one considers the maximum values of T_α allowed by the uncertain Q_α energies are then comparable to $T_{\beta^+/EC}$ in the deformed case. As a consequence, α -decay in this mass region will be always dominant and much faster than β^+/EC -decay.

Finally, Tables 1–3 show the Q_α and Q_{EC} energies, as well as T_α and $T_{\beta^+/EC}$ half-lives for nuclei involved in various α -decay chains starting at ^{295}Og and ^{296}Og (Table 1), $^{295}119$ (Table 2), and $^{295}120$, $^{296}120$, $^{297}120$, and $^{298}120$ (Table 3). The last column stands for the ratios $\mathcal{R} = T_{\beta^+/EC}/T_\alpha$.

Since the SHN produced after neutron evaporation of the corresponding compound nuclei are identified by their α -decay chains, the competition between α and β^+/EC decay modes in the members of a given chain of α -decays is important to analyze possible branching points in future experiments.

Q -energies in the tables are taken from experiment [73] when available, together with their errors within parentheses. Otherwise, they are calculated from the mass formula WS4-RBF [42] and quoted without errors. Similarly, the half-lives are either experimental with errors or calculated with the Q -values given in the tables. In the latter case, T_α corresponds to the average value of the phenomenological parametrizations used earlier, whereas $T_{\beta^+/EC}$ is calculated with the HF+BCS+pnQRPA formalism for the ground states of the nuclei. As it can be seen from the tables, the α -decay mode of a given isotope is generally orders of magnitude faster than the corresponding β^+/EC decay with ratios \mathcal{R} of several orders of magnitude. Nevertheless, \mathcal{R} decreases as we progress in odd- A chains and can reach values close to one at the end of some of these chains. This is the case of nuclei such as ^{267}Sg , ^{265}Rf , ^{267}Db , and ^{263}Lr . However, spontaneous fission becomes

Table 1: Q_α and Q_{EC} energies [MeV], as well as T_α and $T_{\beta^+/EC}$ half-lives [s] for nuclei in the α -decay chains starting at ^{295}Og and ^{296}Og . Available experimental values appear with the errors within parentheses. Otherwise, they are calculated values (see text). The last column contains the ratio $\mathcal{R} = T_{\beta^+/EC}/T_\alpha$

	Q_α	Q_{EC}	T_α	$T_{\beta^+/EC}$	\mathcal{R}
^{295}Og	11.7(9)	4.38	7.1×10^{-3}	2.3×10^3	3.2×10^5
^{291}Lv	10.89(5)	3.4(10)	2.8×10^{-2} (15)	8.1×10^2	2.9×10^4
^{287}Fl	10.16(5)	2.83(95)	5.2×10^{-1} (13)	1.1×10^3	2.1×10^3
^{283}Cn	9.94(11)	2.21(93)	4.1×10^0 (10)	2.2×10^3	5.4×10^2
^{279}Ds	10.08(11)	1.63(90)	2.6×10^{-1}	7.6×10^3	2.9×10^4
^{275}Hs	9.44(5)	0.93(84)	2.9×10^{-1} (15)	4.4×10^4	1.5×10^5
^{271}Sg	8.89(11)	0.16	2.9×10^1	-	-
^{267}Rf	7.89(30)	-0.48	1.2×10^4	-	-
^{296}Og	11.73	2.58	2.3×10^{-3}	4.2×10^2	1.8×10^5
^{292}Lv	10.774(15)	2.33	2.4×10^{-2} (12)	2.7×10^3	1.1×10^5
^{288}Fl	10.072(13)	1.14	7.5×10^{-1} (14)	8.0×10^6	1.1×10^7
^{284}Cn	9.60(20)	0.84	8.1×10^0	6.2×10^6	7.7×10^5

Table 2: Same as in Table 1, but for the α -chain starting at $^{295}119$.

	Q_α	Q_{EC}	T_α	$T_{\beta^+/EC}$	\mathcal{R}
$^{295}119$	12.73	5.79	9.1×10^{-5}	4.8×10^3	5.3×10^7
^{291}Ts	11.5(4)	4.41(85)	1.2×10^{-2}	3.8×10^4	3.2×10^6
^{287}Mc	10.76(5)	3.82(75)	9.5×10^{-2} (60)	3.1×10^3	3.3×10^4
^{283}Nh	10.51(11)	3.22(75)	1.6×10^{-1} (10)	5.3×10^1	3.3×10^2
^{279}Rg	10.52(5)	2.65(73)	1.8×10^{-1} (11)	1.1×10^2	5.9×10^2
^{275}Mt	10.48(5)	2.21(72)	1.17×10^{-1} (74)	5.1×10^3	4.4×10^4
^{271}Bh	9.42(5)	1.16(72)	1.7×10^0	1.4×10^5	8.2×10^4
^{267}Db	7.92(30)	0.63(71)	2.8×10^4	6.2×10^3	2.2×10^{-1}
^{263}Lr	7.68(20)	0.60(57)	3.1×10^4	5.0×10^4	1.6×10^0

the dominant decay mode for them. It is also worth noting that in cases where Q_{EC} is very small, the large $T_{\beta^+/EC}$ obtained are very sensitive to fine details of the calculations because they are determined from the few low-lying transitions located just below Q_{EC} .

As we go forward in a given chain, there is a general trend of decreasing values of the Q_α and Q_{EC} energies, which is translated into increasing half-lives and decreasing ratios. This general trend is somewhat altered in the vicinity of $Z = 112$ and $N = 168$ nuclei, where sub-shell effects are expected at slightly prolate deformations, which are typical of nuclei in this mass region [35].

4. Conclusions

β^+/EC -decay half-lives of some selected even-even and odd- A isotopes in the region of SHN with proton numbers $Z = 118 - 120$ and neutron numbers $N = 175 - 184$ have been studied. $Z = 119$ and 120 are the next elements to be discovered and their production is object of very active experimental campaigns.

Table 3: Same as in Table 1, but for the α -chains starting at $^{295}\text{L20}$, $^{296}\text{L20}$, $^{297}\text{L20}$, and $^{298}\text{L20}$.

	Q_α	Q_{EC}	T_α	$T_{\beta^+/EC}$	\mathcal{R}
$^{295}\text{L20}$	13.25	6.15	1.7×10^{-5}	4.6×10^2	2.7×10^7
^{291}Og	12.39	5.63	2.5×10^{-4}	9.8×10^1	3.9×10^5
^{287}Lv	11.25	4.93	2.5×10^{-2}	7.9×10^1	3.1×10^3
^{283}Fl	10.84	4.15	5.8×10^{-2}	2.4×10^1	4.2×10^2
^{279}Cn	11.04(20)	3.26(62)	4.5×10^{-3}	1.7×10^2	3.8×10^4
^{275}Ds	11.40(30)	2.74(59)	1.0×10^{-2}	8.3×10^2	8.3×10^4
^{271}Hs	9.51(11)	1.82(50)	2.1×10^0	5.3×10^3	2.5×10^3
^{267}Sg	8.63(21)	1.73(49)	2.1×10^2	2.7×10^2	1.3×10^0
^{263}Rf	8.25(15)	1.03(32)	6.7×10^2	2.3×10^5	3.4×10^2
$^{296}\text{L20}$	13.32	4.66	4.6×10^{-6}	4.4×10^1	9.5×10^6
^{292}Og	12.21	3.79	5.0×10^{-4}	1.9×10^2	3.9×10^5
^{288}Lv	11.26	3.30	7.4×10^{-3}	1.2×10^2	1.6×10^4
^{284}Fl	10.83(3)	2.33(85)	3.3×10^{-3} (14)	2.0×10^2	5.9×10^4
$^{297}\text{L20}$	13.12	5.67	2.8×10^{-5}	9.6×10^2	3.4×10^7
^{293}Og	11.9(9)	4.49(107)	2.9×10^{-3}	1.6×10^3	5.5×10^5
^{289}Lv	11.1(3)	3.86(95)	5.6×10^{-2}	1.3×10^3	2.3×10^4
^{285}Fl	10.56(5)	3.27(90)	2.1×10^{-1} (10)	6.7×10^2	3.2×10^3
^{281}Cn	10.45(5)	2.72(89)	1.8×10^{-1} (8)	5.7×10^2	3.2×10^3
^{277}Ds	10.83(11)	2.17(80)	6×10^{-3} (3)	5.0×10^2	8.3×10^4
^{273}Hs	9.70(5)	1.26(78)	1.06×10^0 (50)	1.4×10^4	1.3×10^4
^{269}Sg	8.65(5)	0.61(72)	3.0×10^2 (18)	1.6×10^5	5.3×10^2
^{265}Rf	7.81(30)	0.46(66)	2.5×10^4	2.8×10^4	1.1×10^0
$^{298}\text{L20}$	12.98	3.76	2.0×10^{-5}	2.0×10^2	9.8×10^6
^{294}Og	11.8(7)	2.94(94)	1.2×10^{-3} (5)	1.3×10^2	1.1×10^5
^{290}Lv	11.00(7)	2.30(93)	8×10^{-3} (3)	2.9×10^3	3.6×10^5
^{286}Fl	10.37(3)	1.76(93)	2.8×10^{-1}	4.8×10^3	1.7×10^4

The nuclear structure of the decay partners is described microscopically within a pnQRPA based on a self-consistent deformed Skyrme HF+BCS approach. Uncertainties in the Q -energies originated from the unknown masses are translated into uncertainties in the half-lives calculated with them. We have used different mass formulas to evaluate the expected spread on the half-lives. The results for $T_{\beta^+/EC}$ are compared with those of T_α obtained from several phenomenological formulas using Q_α energies obtained from the same mass formulas. The T_α half-lives are systematically lower than the corresponding $T_{\beta^+/EC}$ ones for a given isotope. The difference is always larger than three orders of magnitude in the most favored case of deformed nuclei and becomes much larger for the spherical ground states. Therefore, the β^+/EC -decay mode will hardly compete with α -decay in the SHN studied with $Z=118, 119$, and 120 .

The competition between α and β^+/EC decay modes is also studied in seven α -decay chains starting at different isotopes of $Z=118, 119$, and 120 . The ratio of half-lives for both modes indicates that α -decay is generally several orders of magnitude (up to seven orders in the chain heads) faster than β^+/EC -decay. However, the half-lives become comparable at the end of some of the chains studied. Hence, the cases in which different decay branches are more likely to appear have been identified. This could be

useful as a theoretical guide for future experimental studies of these decays in new elements not yet discovered.

Acknowledgments

I would like to thank G. G. Adamian for useful discussions and valuable advice. This work was supported by Ministerio de Ciencia e Innovación MCI/AEI/FEDER,UE (Spain) under Contract No. PGC2018-093636-B-I00.

References

References

- [1] S. Hofmann, G. Münzenberg, Rev. Mod. Phys. 72 (2000) 733.
- [2] J.H. Hamilton, D. Hofmann, Y.T. Oganessian, Annu. Rev. Nucl. Part. Sci. 63 (2013) 383.
- [3] Yu. Ts. Oganessian, V.K. Utyonkov, Rep. Prog. Phys. 78 (2015) 036301.
- [4] S. Hofmann, et al., Eur. Phys. J. A 52 (2016) 180.
- [5] S.A. Giuliani, et al., Rev. Mod. Phys. 91 (2019) 011001.
- [6] K. Morita, et al., J. Phys. Soc. Japan 73(10) (2004) 2593.
- [7] Yu. Ts. Oganessian, et al., Phys. Rev. C 69 (2004) 021601(R).
- [8] Yuri Oganessian, J. Phys. G: Nucl. Part. Phys. 34 (2007) R165.
- [9] Yu. Ts. Oganessian, V.K. Utyonkov, Nucl. Phys. A 944 (2015) 62.
- [10] S.G. Nilsson, et al., Nucl. Phys. A 115 (1968) 545.
- [11] P. Möller, J.R. Nix, J. Phys. G: Nucl. Part. Phys. 20 (1994) 1681.
- [12] A.N. Kuzmina, G.G. Adamian, N.V. Antonenko, W. Scheid, Phys. Rev. C 85 (2012) 014319.
- [13] K. Rutz, et al., Phys. Rev. C 56 (1997) 238.
- [14] A.T. Kruppa, M. Bender, W. Nazarewicz, P.-G. Reinhard, T. Vertse, S. Ćwiok, Phys. Rev. C 61 (2000) 034313.
- [15] M. Bender, W. Nazarewicz, P.-G. Reinhard, Phys. Lett. B 515 (2001) 42.
- [16] J. Meng, H. Toki, S.G. Zhou, S.Q. Zhang, W.H. Long, L.S. Geng, Prog. Part. Nucl. Phys. 57 (2006) 470.
- [17] S.E. Agbemava, A.V. Afanasjev, T. Nakatsukasa, P. Ring, Phys. Rev. C 92 (2015) 054310.
- [18] A. Lopez-Martens, et al., Phys. Lett. B 795 (2019) 271.
- [19] F.P. Heßberger, Eur. Phys. J. A 55 (2019) 208.
- [20] Juhee Hong, G.G. Adamian, N.V. Antonenko, Phys. Rev. C 94 (2016) 044606; Phys. Lett. B 764 (2017) 42.
- [21] G.G. Adamian, N.V. Antonenko, A. Diaz-Torres, S. Heinz, Eur. Phys. J. A 56 (2020) 47.
- [22] G.G. Adamian, N.V. Antonenko, W. Scheid, Phys. Rev. C 69 (2004) 044601.
- [23] H.M. Albers, et al., Phys. Lett. B 808 (2020) 135626.
- [24] G.G. Adamian, N.V. Antonenko, H. Lenske, L.A. Malov, Phys. Rev. C 101 (2020) 034301.
- [25] A. Baran, M. Kowal, P.-G. Reinhard, L.M. Robledo, A. Staszczak, and M. Warda, Nucl. Phys. A 944 (2015) 442.
- [26] A.V. Karpov, V.I. Zagrebaev, Y. Martinez Palazuela, L. Felipe Ruiz, Walter Greiner, Int. J. Mod. Phys. E 21 (2012) 1250013.
- [27] V.I. Zagrebaev, A.V. Karpov, Walter Greiner, Phys. Rev. C 85 (2012) 014608.
- [28] F.P. Heßberger, et al., Eur. Phys. J. A 52 (2016) 328.
- [29] J. Khuyagbaatar, et al., Phys. Rev. Lett. 125 (2020) 142504.
- [30] X. Zhang, Z. Ren, Phys. Rev. C 73 (2006) 014305.
- [31] E.O. Fiset, J.R. Nix, Nucl. Phys. A 193 (1972) 647.
- [32] U.K. Singh, P.K. Sharma, M. Kaushik, S.K. Jain, Dashty T. Akraway, G. Saxena, Nucl. Phys. A 1004 (2020) 122035.
- [33] P. Möller, M.R. Mumpower, T. Kawano, W.D. Myers, At. Data Nucl. Data Tables 125 (2019) 1.
- [34] P. Sarriguren, Phys. Rev. C 100 (2019) 014309.
- [35] P. Sarriguren, J. Phys. G: Nucl. Part. Phys. 47 (2020) 125107.

- [36] P. Sarriguren, E. Moya de Guerra, A. Escuderos, A. C. Carrizo, Nucl. Phys. A 635 (1998) 55.
- [37] P. Sarriguren, E. Moya de Guerra, A. Escuderos, Nucl. Phys. A 658 (1999) 13; Nucl. Phys. A 691 (2001) 631; Phys. Rev. C 64 (2001) 064306.
- [38] C.F. von Weizsacker, Z. Phys. 96 (1935) 431 (1935); H.A. Bethe, R.F. Bacher, Rev. Mod. Phys. 8 (1936) 829.
- [39] P. Möller, A.J. Sierk, T. Ichikawa, H. Sagawa, At. Data Nucl. Data Tables 109-110 (2016) 1.
- [40] H. Koura, T. Tachibana, M. Unos, N. Yamada, Prog. Theor. Phys. 113 (2005) 305.
- [41] J. Duflo, A.P. Zuker, Phys. Rev. C 52 (1995) R23; J. Mendoza-Temis, J.G. Hirsch, A.P. Zuker, Nucl. Phys. A 843 (2010) 14.
- [42] N. Wang, M. Liu, X.Z. Wu, J. Meng, Phys. Lett. B 734 (2014) 215.
- [43] Y.Z. Wang, S.J. Wang, Z.Y. Hou, J.Z. Gu, Phys. Rev. C 92 (2015) 064301.
- [44] M.V. Stoitsov, J. Dobaczewski, W. Nazarewicz, S. Pittel, D.J. Dean, Phys. Rev. C 68 (2003) 054312.
- [45] M. V. Stoitsov, J. Dobaczewski, W. Nazarewicz, P. Ring, Comp. Phys. Comm. 167 (2005) 43.
- [46] <https://www.fuw.edu.pl/~dobaczew/thodri/thodri.html>;
www.nuclearmasses.org
- [47] N.B. Gove, M.J. Martin, Nucl. Data Tables 10 (1971) 205.
- [48] M.J. Martin and P.H. Blichert-Toft, Nuclear Data Tables A 8 (1970) 1.
- [49] S. Stoica, M. Mirea, O. Niuescu, J.U. Nabi, and M. Ishfaq, Adv. High En. Phys. 2016 (2016) 8729893;
M. Ishfaq, J.U. Nabi, O. Niuescu, M. Mirea, and S. Stoica, Adv. High En. Phys. 2019 (2019) 5783618.
- [50] X. Mougeot, Appl. Radiat. Isot. 134 (2018) 225; 154 (2019) 108884.
- [51] E. Chabanat, P. Bonche, P. Haensel, J. Meyer, R. Schaeffer, Nucl. Phys. A 635 (1998) 231.
- [52] D. Vautherin, D.M. Brink, Phys. Rev. C 5 (1972) 626; D. Vautherin, Phys. Rev. C 7 (1973) 296.
- [53] S. Hilaire, M. Girod, Eur. Phys. J. A 33 (2007) 237;
www-phynu.cea.fr/science_en_ligne/carte_potentiels_micropotentiels/carte_potentiel_nucleaire_eng.htm
- [54] N. Schunck, et al., Phys. Rev. C 81 (2010) 024316.
- [55] P. Sarriguren, R. Alvarez-Rodríguez, E. Moya de Guerra, Eur. Phys. J. A 24 (2005) 193.
- [56] P. Sarriguren, Phys. Rev. C 79 (2009) 044315; Phys. Lett. B 680 (2009) 438; Phys. Rev. C 83 (2011) 025801.
- [57] P. Sarriguren, O. Moreno, R. Alvarez-Rodríguez, E. Moya de Guerra, Phys. Rev. C 72 (2005) 054317.
- [58] O. Moreno, P. Sarriguren, R. Alvarez-Rodríguez, E. Moya de Guerra, Phys. Rev. C 73 (2006) 054302.
- [59] J.M. Boillos, P. Sarriguren, Phys. Rev. C 91 (2015) 034311.
- [60] P. Sarriguren, J. Pereira, Phys. Rev. C 81 (2010) 064314.
- [61] P. Sarriguren, A. Algora, J. Pereira, Phys. Rev. C 89 (2014) 034311.
- [62] P. Sarriguren, Phys. Rev. C 91 (2015) 044304.
- [63] P. Sarriguren, A. Algora, G. Kiss, Phys. Rev. C 98 (2018) 024311.
- [64] P. Sarriguren, Phys. Rev. C 95 (2017) 014304.
- [65] P. Sarriguren, E. Moya de Guerra, R. Alvarez-Rodríguez, Nucl. Phys. A 716 (2003) 230.
- [66] P. Sarriguren, Phys. Rev. C 87 (2013) 045801; Phys. Rev. C 93 (2016) 054309.
- [67] E. Náchter, et al., Phys. Rev. Lett. 92 (2004) 232501.
- [68] A. Parkhomenko, A. Sobiczewski, Acta Physica Polonica B 36 (2005) 3095.
- [69] G. Royer, J. Phys. G: Nucl. Part. Phys. 26 (2000) 1149.
- [70] V.E. Viola, Jr., G.T. Seaborg, J. Inorg. Nucl. Chem. 28 (1966) 741.
- [71] A. Sobiczewski, Z. Patyk, S. Cwiok, Phys. Lett. B 224 (1989) 1.
- [72] Jun-Gang Deng, Hong-Fei Zhang, G. Royer, Phys. Rev. C 101 (2020) 034307.
- [73] G. Audi, F.G. Kondev, M. Wang, W.J. Huang, S. Naimi, Chinese Physics C 41 (2017) 030001; M. Wang, G. Audi, F.G. Kondev, W.J. Huang, S. Naimi, X. Xu, Chinese Physics C 41 (2017) 030003.